Electrical Engineering (2024) 106:1533–1547
https://doi.org/10.1007/s00202-023-01904-5

ORIGINAL PAPER

Analytical model for double-sided linear permanent magnet inner armature synchronous machine with slot-less stator at on-load in different patterns of magnetization

Ehsan Shirzad[1]

Received: 17 September 2022 / Accepted: 14 June 2023 / Published online: 27 July 2023

Abstract
In this paper is presented a two-dimension analytical model for linear permanent magnet inner armature double-sided synchronous motors (LPMIADSSMs). The flux density in all areas of the proposed machine is calculated based on the sub-domain method. According to this method, the machine areas are divided into eleven sub-regions such as first external, first mover, first PM, first air gap, first winding, stator, second winding, second air gap, second PM, second external and second mover, which sign as FE, FR, FP, FAG, FW, S, SW, SAG, SP, SE and SR. To find the flux density equations, it is mandatory to solve the extracted Maxwell equations and apply the boundary conditions between each two sub-regions, which lead to find the unknown coefficients for flux density in each sub-region. In addition, the influences of magnetization patterns, i.e., parallel, ideal Hal Bach, 2-segment Halbach and bar magnet in the shifting direction of the flux distribution and armature reaction (AR), are investigated. To validate the obtained results, the proposed model results are compared with those obtained from finite element method (FEM) and Maxwell software.

Keywords Linear permanent magnet motor · Analytic model · Flux density · Finite element method · Magnetization patterns · Boundary condition · Double-sided · Coreless

List of symbols

A	Magnetic vector potential (V.s/m).
B	Magnetic flux density vector (T).
B_{rem}	Permanent magnet residual flux density (T).
H	Magnetic field intensity vector (A/m).
J	Armature current density vector (A/m2).
M	Magnetization vector (A/m).
P	Number of pole-pairs.
μ_0	Free space permeability (H/m).
μ_r	Relative permeability.
μ_{rpm}	Relative permeability of permanent magnet
n	Harmonic order

✉ Ehsan Shirzad
ehsan_shirzad_72@yahoo.com

[1] University of Bojnord, Bojnurd, Iran

1 Introduction

Linear permanent magnet motors (LFPMMs) are used in different fields such as flywheel energy storage system, hybrid vehicle system (HEVs), wind turbines, and medical and domestic applications. Moreover, LFPMMs are inherently suitable for high-performance applications, i.e., direct-drive systems and where low noise and smooth torque are imperative requirements [1–4]. Generally, LFPMMs are divided into single-sided, double-sided and multi-stage motors. Radii of stator and rotor and existing of teeth for stator compose special types of LFPMMs. Single-sided structures are used less than double-sided structures because double-sided structures have some advantages rather than single-sided, such as the output energy can be increased to twice compared with the single-sided linear flux machines. In addition, double-sided structure for LFPMM produces an equilibrium force in the center of motor and obstacles vibration and distortion in the middle of this motor building. Figure 1 shows LPMIADSSM that involved in cored and coreless structure. Eliminating cores lead to reduce the core loss and machine volume; therefore, coreless structures are preferred compared

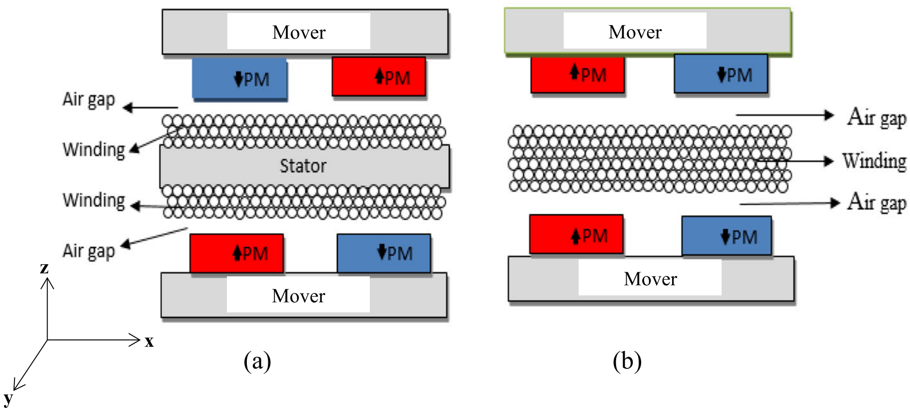

Fig. 1 Cross section of LPMIADSSM: **a** cored **b** coreless

Table 1 Components of the magnetization patterns

Magnetization patterns	Illustrative representation	Tangential components	Normal component	Tangential-Fourier series coefficients: m_{xn}	Perpendicular-Fourier series coefficients: m_{yn}
Parallel	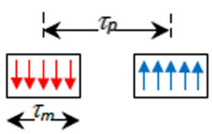	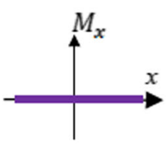	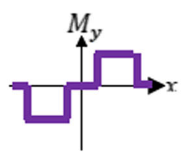	0	$\frac{4B_{rem}}{\mu_0 n\pi}\sin(\frac{n\pi}{2})\times \sin(\frac{\alpha_n\tau_m}{2})$
Ideal Halbach	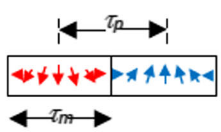	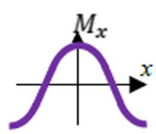	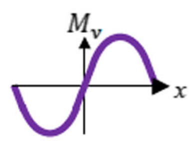	$\begin{cases}\frac{B_{rem}}{\mu_0} & for\ n=1\\ 0 & otherwise\end{cases}$	$\begin{cases}\frac{B_{rem}}{\mu_0} & for\ n=1\\ 0 & otherwise\end{cases}$
2-segment Halbach	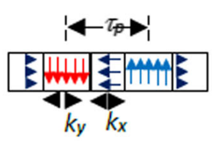	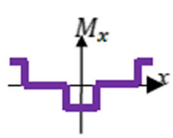	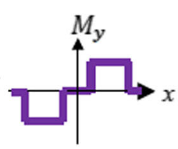	$-\frac{4B_{rem}}{\mu_0 n\pi}\sin\left(\frac{n\pi k_x}{2}\right)$	$\frac{-2B_{rem}}{\mu_0 n\pi}\times\left[\cos\left(n\pi(\frac{k_x}{2}+k_y)\right)-\cos\left(\frac{n\pi k_x}{2}\right)\right]$
Bar magnets in shifting directions	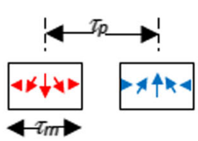	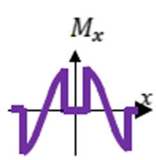	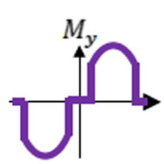	$\begin{cases}-\frac{4n\alpha_p^2B_{rem}}{\mu_0\pi}\frac{\sin\left(\frac{n\pi}{2}\right)\cos\left(\frac{n\pi\alpha_p}{2}\right)}{1-(n\alpha_p)^2} & n\alpha_p\neq1\\ \frac{-B_{rem}}{n\mu_0} & n\alpha_p=1\end{cases}$	$\begin{cases}\frac{4n\alpha_p^2B_{rem}}{\mu_0\pi}\frac{\sin\left(\frac{n\pi}{2}\right)\cos\left(\frac{n\pi\alpha_p}{2}\right)}{1-(n\alpha_p)^2} & n\alpha_p\neq1\\ \frac{B_{rem}}{n\mu_0} & n\alpha_p=1\end{cases}$

with cored structures, and in this paper, the coreless structure is considered; however, this method presented in this paper can be implemented for cored structure.

Analytical model based on sub-domain method is a fast, proven and accurate model; in industrial applications, it is faster than numeric models and are more significant for reducing the time of simulations, which have the same accuracy as the numeric method; this analysis facilitates evaluating the arbitrary motor in different geometric structure values; therefore, analytical models are suggested because they are faster than numeric model and this method can help the users to understand all of interplays in motor, opposite of numerical method that everything is vague and user cannot have a deep realization of the motor behavior and the output results depend on the mesh sizes. The sub-domain method is one of the useful analytic methods investigated in this paper [5–8]. In this method, all the machine areas are divided into an appropriate sub-region and the partial differential equations (PDEs) in each sub-region are defined according to the Maxwell equations. Based on superposition method, the flux density for each sub-region is obtained by considering the PMs and armature current effects separately. Some articles used the analytical model for considering only PMs' excitation (open-circuit mode) [9–11] and some other ones considered only armature reaction (AR) effects [12], and in more accurate analysis both of them has been considered [13–16] (Table 1).

To obtain the accurate results, permeability for cores should not be infinite, and infinite permeability lead to obtain zero magnetic field intensity. It means that there is no any reduction of magneto-motive force in length of flux path in the cores that considers infinite permeability for cores [17], but the proposed method in this article is able to take an account finite permeability for cores and its effect on the flux distribution. Different magnetization patterns are used in the permanent magnet machines that in previous studies parallel magnetization pattern has been reported in some articles [18–21] and Halbach magnetization patterns in [22]. In the previous papers, they have not been concentrated on whole state magnetization [23–26], but in this article whole different arrays of magnetization are considered and calculated.

For summarizing the analytical method in this paper, it can be mentioned that this paper considers finite permeability for cores, variety magnetization patterns and both PM and AR effects on the magnetic flux density.

For reminding, this paper is divided to five sections; in section I have been presented past works. In section II the 2-D analytical model of linear permanent magnet synchronous motor with double mover, assumptions and reasonings for solution problem is expressed and subsections of this part explains proposed motor and calculates mentioned parameters at above. In section III, the presented results of analytical model are compared with FEA model (numerical solution). In the last part is brought concluded explanation of whole article.

2 Methodology and assumptions

At the first step of solution, some assumptions are considered as follows:

- End effects are ignored, i.e., the motor is assumed to have infinite axial length.
- The magnetic flux density has only vertical and horizontal components; this implies that the magnetic vector potential has only axial component.
- All the materials are isotropic.
- The all media have finite permeability.
- The motor has slot-less stator structure.
- The airspace between the magnets has the same permeability as the magnets.
- Eddy current reaction field is neglected.

For obtaining the PDEs in each sub-region in the LPMI-ADSSMs, the investigated algorithm is demonstrated as follows:

- Utilized the assumptions as mentioned.
- Dividing the motor area to the appropriate sub-domain.
- By Poisson and Laplace equation, PDEs of system are introduced.
- For obtaining the unknown constants coefficients in the magnetic flux density, boundary conditions are applied.
- Calculating the expansion Fourier for the current density in the winding sub-region and PM magnetization patterns for obtaining the Poisson equations.
- After knowing constant coefficient for each sub-region, the magnetic flux density is able to be calculated.
- Comparison between the obtained analytic method results and FEM results is made to validate the model.

2.1 Finding the PDEs in each sub-regions

Figure 2 divides different regions for the LPMIADSSMs; in fact, the winding is in direction of y and magnetization patterns of PMS are in the z and x directions.

The simplified Maxwell equation, which is applied to each sub-region to find the magnetic vector potential, is shown in Eq. 1.

$$-\nabla^2 \boldsymbol{A}_y^i = \mu_r \boldsymbol{J}_y^i + \mu_0 \nabla \times \boldsymbol{M} \quad (1)$$

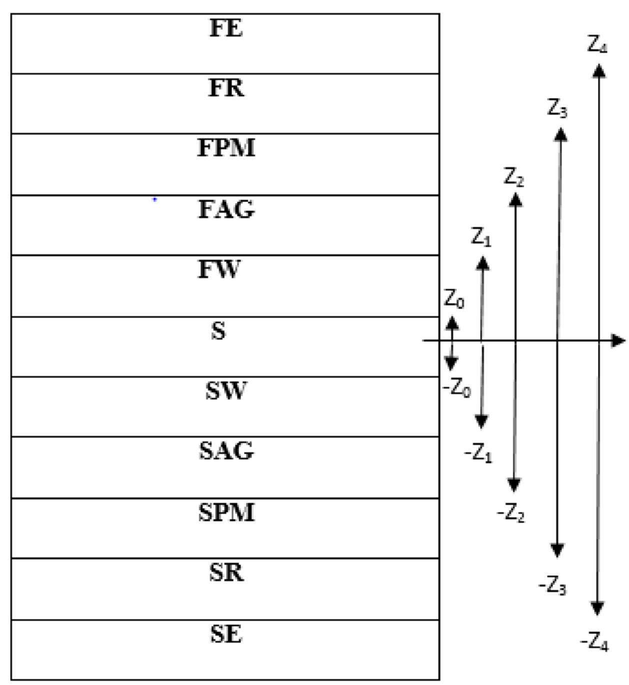

Fig. 2 Dividing of LPMIADSSMs

Table 2 Boundary conditions for intersection of regions

Boundary conditions in vertical component	Boundary conditions in horizontal component
$B_z^{FE}(x, Z_4) = B_z^{FR}(x, Z_4)$	$H_x^{FE}(x, Z_4) = H_x^{FR}(x, Z_4)$
$B_z^{FR}(x, Z_3) = B_z^{FPM}(x, Z_3)$	$H_x^{FR}(x, Z_3) = H_x^{FPM}(x, Z_3)$
$B_z^{FPM}(x, Z_2) = B_z^{FAG}(x, Z_2)$	$H_x^{FPM}(x, Z_2) = H_x^{FAG}(x, Z_2)$
$B_z^{FAG}(x, Z_1) = B_z^{FW}(x, Z_1)$	$H_x^{FAG}(x, Z_1) = H_x^{FW}(x, Z_1)$
$B_z^{FW}(x, Z_0) = B_z^{S}(x, Z_0)$	$H_x^{FW}(x, Z_0) = H_x^{S}(x, Z_0)$
$B_z^{S}(x, -Z_0) = B_z^{SW}(x, -Z_0)$	$H_x^{S}(x, -Z_0) = H_x^{SW}(x, -Z_0)$
$B_z^{SW}(x, -Z_1) = B_z^{SAG}(x, -Z_1)$	$H_x^{SW}(x, -Z_1) = H_x^{SAG}(x, -Z_1)$
$B_z^{SAG}(x, -Z_2) = B_z^{SPM}(x, -Z_2)$	$H_x^{SAG}(x, -Z_2) = H_x^{SPM}(x, -Z_2)$
$B_z^{SPM}(x, -Z_3) = B_z^{SR}(x, -Z_3)$	$H_x^{SPM}(x, -Z_3) = H_x^{SR}(x, -Z_3)$
$B_z^{SR}(x, -Z_4) = B_z^{SE}(x, -Z_4)$	$H_x^{SR}(x, -Z_4) = H_x^{SE}(x, -Z_4)$

It is noted that in the PM sub-region $J = 0$, in the winding sub-region $M = 0$ and for other regions both of J and M are zero. Based on solving differential equation method, it is necessary to find the homogeneous solution for (1). To achieve this aim, separation variables are applied; therefore, in the i = FAG, SAG, FE, SE, FR, SR, S, the magnetic vector potential is obtained as follows that $\alpha_n = n\pi/\tau_p$ where τ_p is pole pitch.

$$-\nabla^2 \boldsymbol{A}_y^i = 0 \tag{2}$$

$$\boldsymbol{A}_y^i(x, z) = \sum_{n=1}^{\infty} \left(a_n^i sinh(\alpha_n z) + b_n^i \cosh(\alpha_n z)\right) cos(\alpha_n x) + \left(c_n^i sinh(\alpha_n z) + d_n^i \cosh(\alpha_n z)\right) sin(\alpha_n x) \tag{3}$$

Magnetic flux density is obtained for each sub-region by using curl from magnetic vector potential ($B = \nabla \times A$); component of horizontal and z is obtained:

$$B_x^i(x, z) = \frac{\partial A_y^i}{\partial z} \tag{4}$$

$$B_z^i(x, z) = \frac{-\partial A_y^i}{\partial x} \tag{5}$$

Table 3 Specifications of studied LPMIADSSM

Parameters	Values
Stator back iron height, $2Z_0$	20 mm
Winding region height, Z_1-Z_0	8 mm
Air gap region height, Z_2-Z_1	2 mm
Mover back iron height, Z_4-Z_3	10 mm
Number of poles	4
Embrace, τ_m/τ_p	0.8
Relative permeability in space, μ_0	0.000001256
Relative permeability in permanent magnet, μ_{rpm}	1.23
Magnetic field intensity in Permanent magnet, M	979,299.36A.t/m
Relative permeability in iron, M_r	1000
Current density, J	$1A/mm^2$
Filling factor,K_f	0.5

Strength field in (7), (8) is written:

$H_x^i = \frac{B_x^i}{\mu_0 \mu_r^i} - \frac{M}{\mu_r^i}$ (6) For regions winding Fw and SW that after solving Eq. 7, relation 8 will occur.

$$-\nabla^2 \boldsymbol{A}_y^i = -\mu_0 \boldsymbol{J}_y^i \tag{7}$$

$$A_y^i(x, z) = \sum_{n=1}^{\infty} \left(a_n^i sinh(\alpha_n z) + b_n^i \cosh(\alpha_n z) + \mu_0 J_{2n}/\alpha_i^2\right) cos(\alpha_n x) + \left(c_n^i sinh(\alpha_n z) + d_n^i \cosh(\alpha_n z) + \mu_0 J_{1n}/\alpha_i^2\right) sin(\alpha_n x) \tag{8}$$

where Fourier expansion for current density in winding region is:

$$\boldsymbol{J}_y^i(x, t) = \sum_{n=1}^{\infty} J_{1n} sin(\alpha_n x) + J_{2n} cos(\alpha_n x) \tag{9}$$

For FPM and SPM, the relation similar to other regions is written:

$$-\nabla^2 \boldsymbol{A}_y^i = \mu_0 \nabla \times \boldsymbol{M} \tag{10}$$

Magnetic vector potential is the sum of private and general answer, but there is a difference in other regions, because the PMs and movers move; therefore x changes to x_{new} where v shows the linear velocity of movers and PMs:

$$x_{new} = x - d \tag{11}$$

That:

$$d = vt + d_0 \tag{12}$$

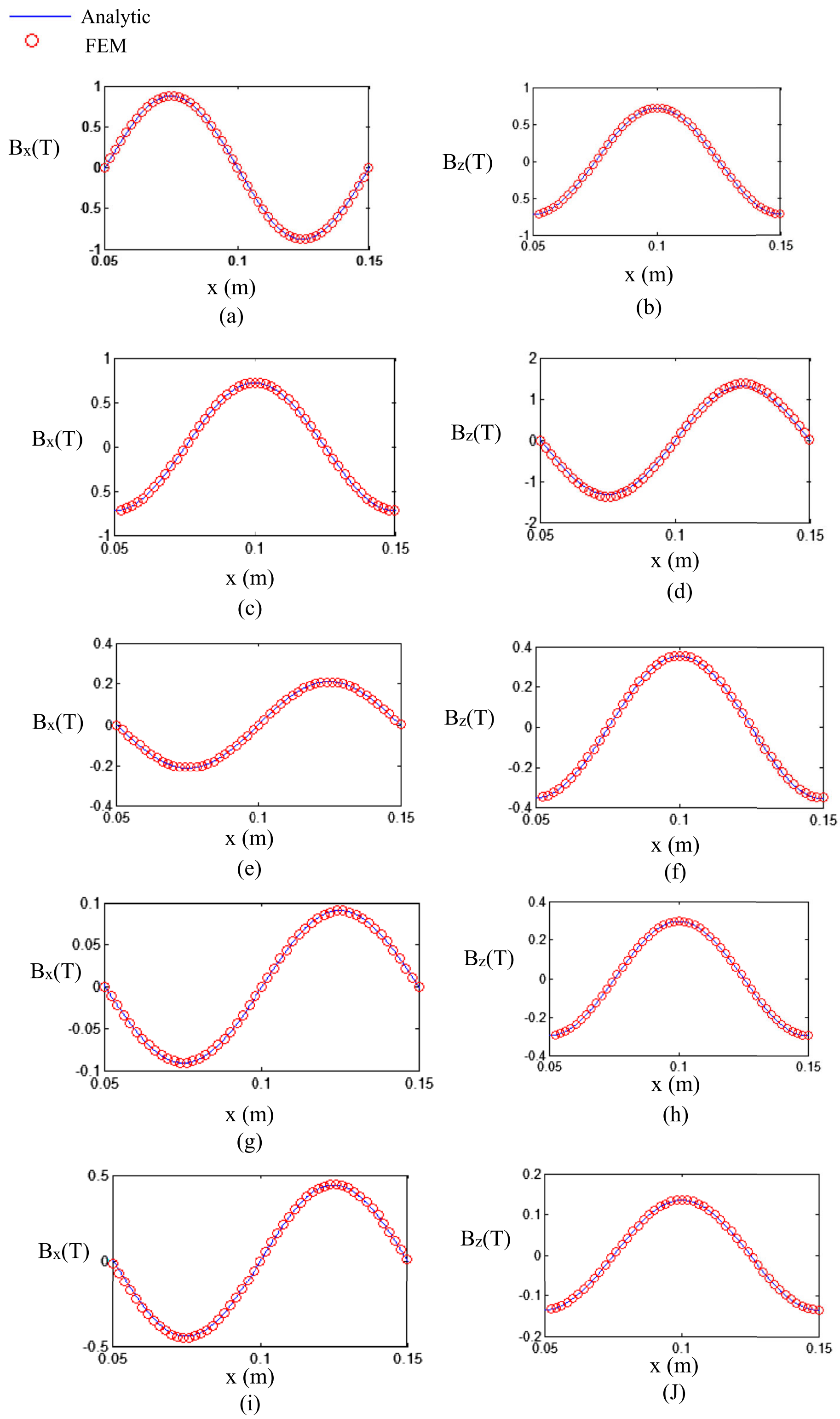

Fig. 3 Distribution of flux density for ideal Halbach magnetization: **a** Flux density horizontal component of FR, **b** flux density vertical component of FR, **c** flux density horizontal component of FPM, **d** flux density vertical component of FPM, **e** flux density horizontal component of FAG, **f** flux density vertical component of FAG, **g** flux density horizontal component of FW, **h** flux density vertical component of FW, **I** flux density horizontal component of S, **J** flux density vertical component of S, **k** flux density horizontal component of SW, **L** flux density vertical component of SW, **m** flux density horizontal component of SAG, **n** flux density vertical component of SAG, **o** flux density horizontal component of SPM, **p** flux density vertical component of SPM, **Q** flux density horizontal component of SR, **R** flux density vertical component of SR

Fig. 3 continued

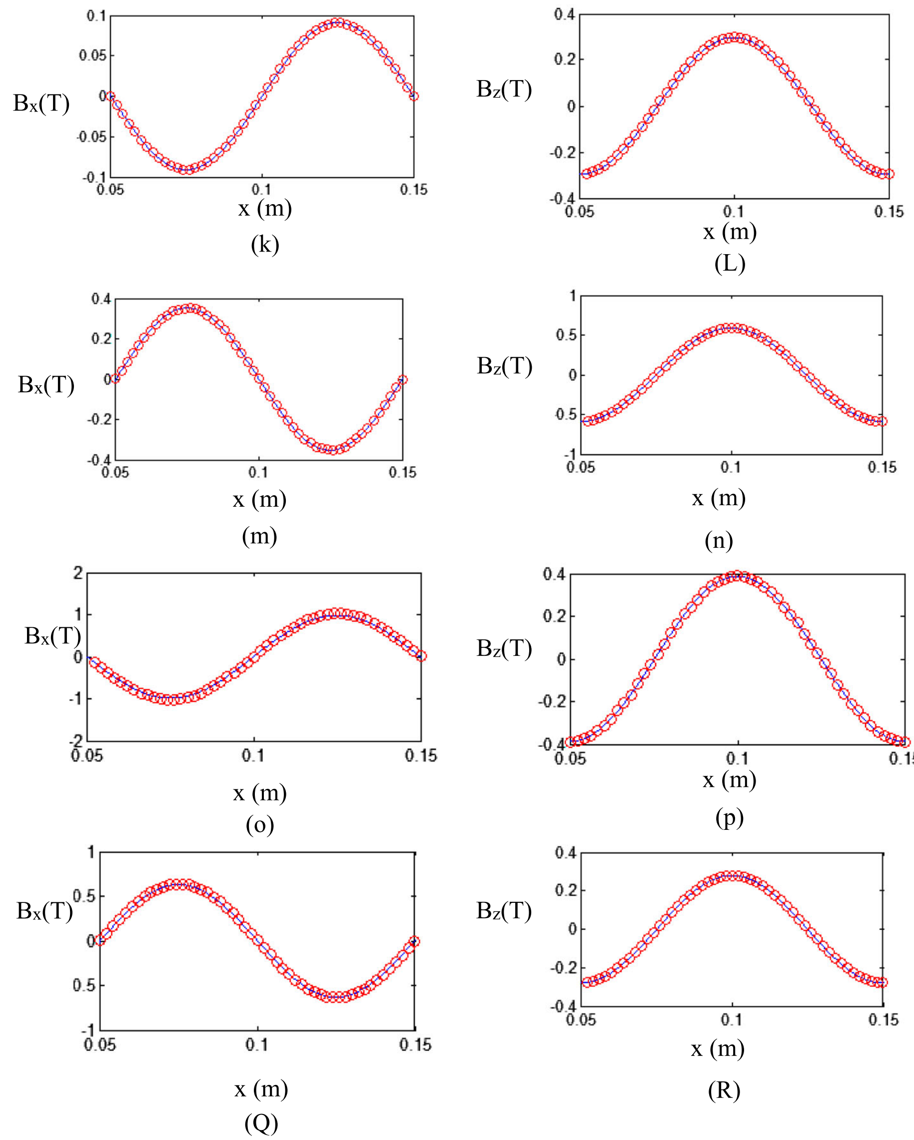

Corresponding to mentioned procedure, for magnetic potential vector in FPM and SPM we have:

$$A_y^i(x, z) = \sum_{n=1}^{\infty} \left(a_n^i \sinh(\alpha_n z) + b_n^i \cosh(\alpha_n z) + \mu_0 J_{2n}/\alpha_i^2 \right) \cos(\alpha_n x) + \left(c_n^i \sinh(\alpha_n z) + d_n^i \cosh(\alpha_n z) + \mu_0 J_{1n}/\alpha_i^2 \right) \sin(\alpha_n x) \tag{13}$$

where vector of **M** is extracted from Fourier expansion of shape of magnetization with respect to displacement:

$$\boldsymbol{M} = \sum_{n=1}^{\infty} m_{xn} cos(\alpha_n x) + m_{yn} sin(\alpha_n x) \tag{14}$$

Each sub-region has 4 unknown variables, which by applying the boundary conditions is similar to Table 2, in intersection between each two sub-regions; this variable can be found. Boundary conditions clarify that vertical components of the magnetic flux density and horizontal components of magnetic field intensity must be continued in the intersection of two sub-regions as:

3 Flux density distribution due to PM and AR

The simulations were obtained in the presence of winding and PM conditions separately. Firstly, the flux density due to PM in all of regions will be calculated and compared with the results of FEM.

The horizontal and vertical components of flux density according to Table 3 at the center of each-region for the different magnetization are shown in different figures that all the evaluations are done in static model and at the special

Fig. 4 Distribution of flux density for two-segment Halbach magnetization: **a** Flux density horizontal component of FR, **b** Flux density vertical component of FR, **c** Flux density horizontal component of FPM, **d** Flux density vertical component of FPM, **e** Flux density horizontal component of FAG, **f** Flux density vertical component of FAG, **g** Flux density horizontal component of FW, **h** Flux density vertical component of FW, **I** Flux density horizontal component of S, **J** Flux density vertical component of S, **k** Flux density horizontal component of SW, **L** Flux density vertical component of SW, **m** Flux density horizontal component of SAG, **n** Flux density vertical component of SAG, **o** Flux density horizontal component of SPM, **p** Flux density vertical component of SPM, **Q** Flux density horizontal component of SR, **R** Flux density vertical component of SR

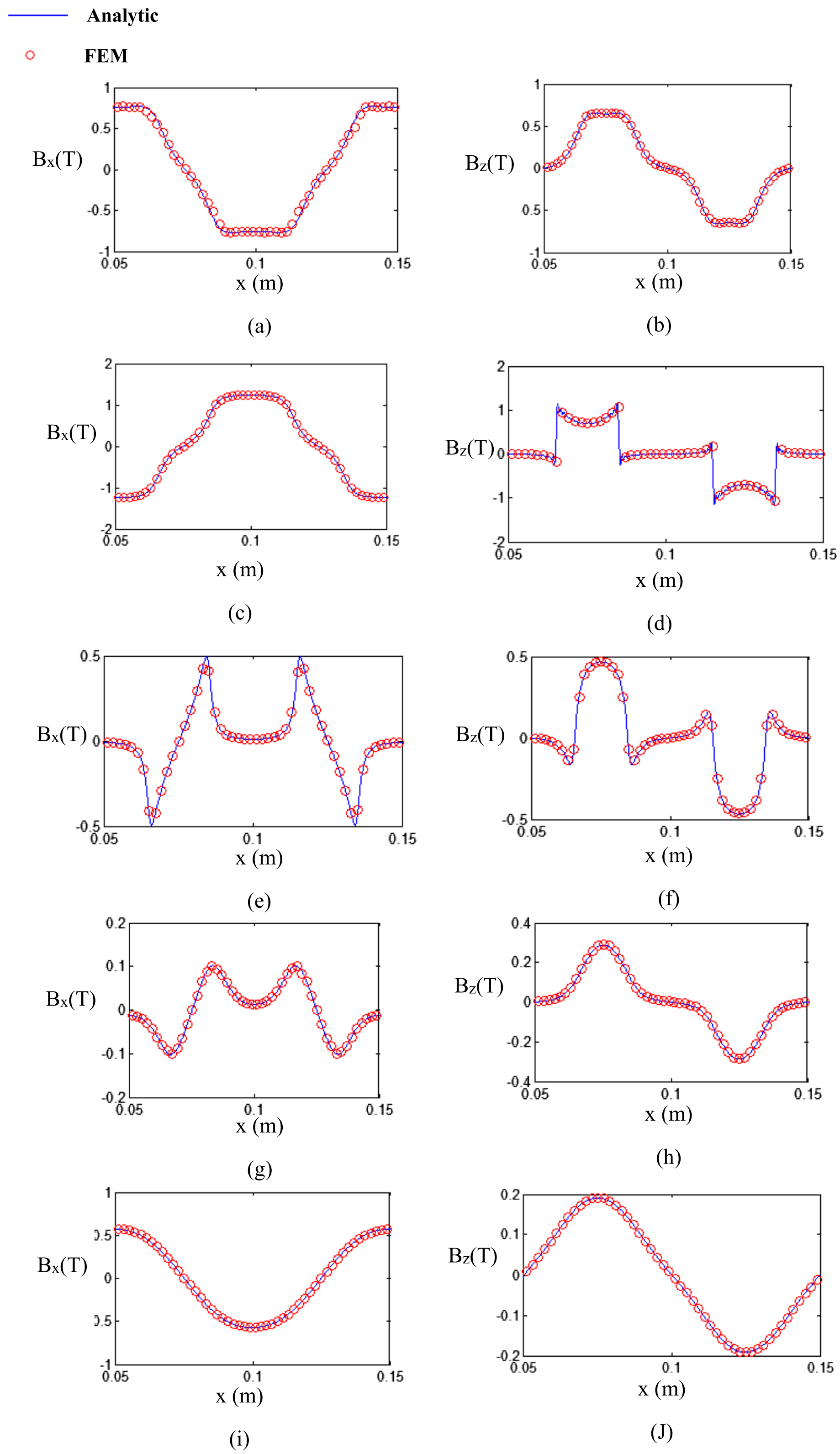

Fig. 4 continued

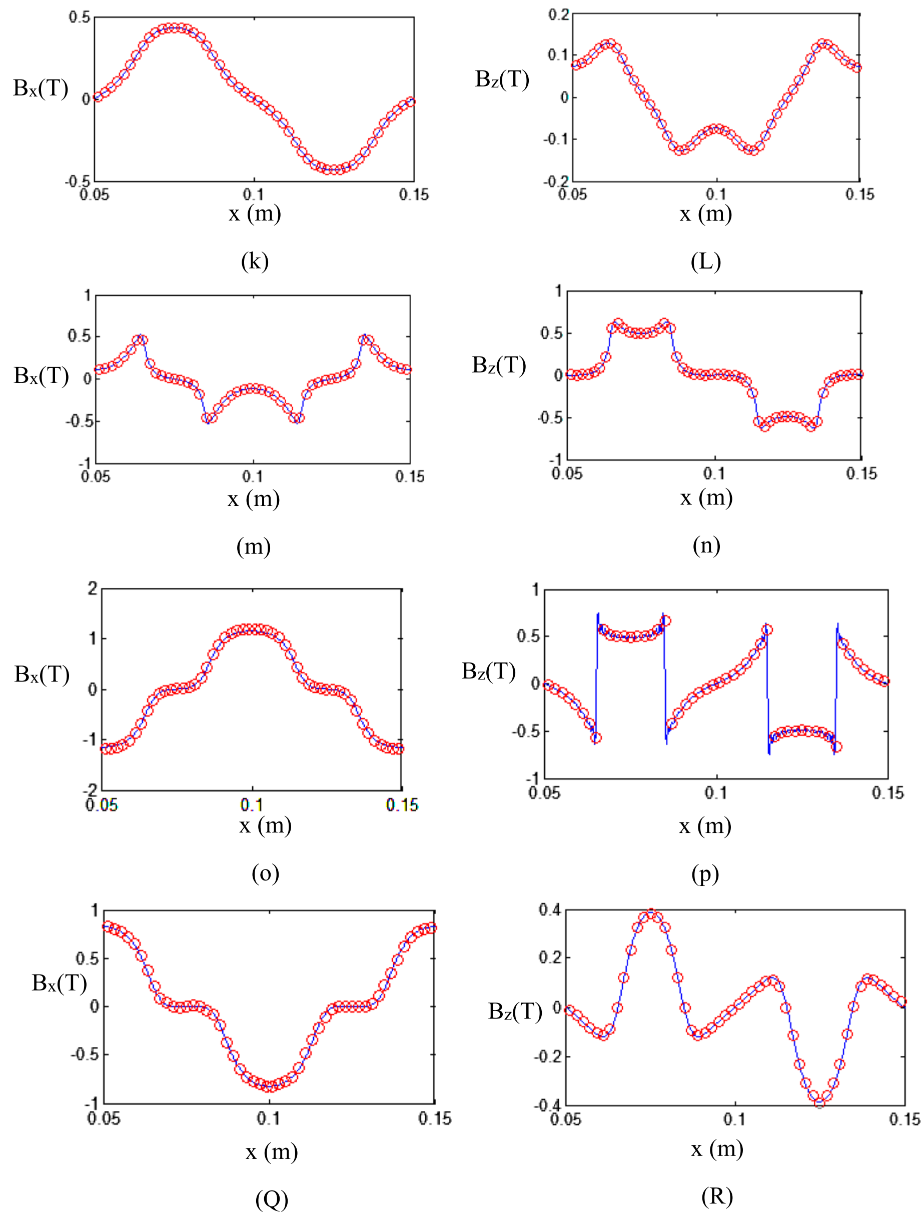

time. Simulated results for analytic model and FEM in all the regions for ideal Halbach pattern are illustrated in Fig. 3, two-segment Halbach pattern in Fig. 4, parallel pattern in Fig. 5 and bar magnet in the shifting direction pattern in Fig. 6 for horizontal and vertical component; moreover, this motor is examined when there's only winding and neglects the effect of PM; therefore, for each region results of FEM and analytical method in Fig. 7 are compared together. Finally, superposition theory can be used to calculate the effect of either PM or winding at the same time. The interesting point in the three Halbach magnetization patterns is related to the magnetic flux path that it passes mainly through the PMs and the magnetic flux in the rotor is negligible, and it is possible to replace the rotor with other material having less weight, less volume and cheaper than the ferromagnetic materials. Also, it is evident that the ideal Halbach magnetization includes less THD compared with other magnetization patterns.

Another exciting point in the simulation procedure is related to the time of the simulation that for the analytical model it is 14 times less than the numerical one. It means in the design stage optimization problem includes too many iterations, and times can be saved by implementing the analytical model, if possible, instead of the numerical model.

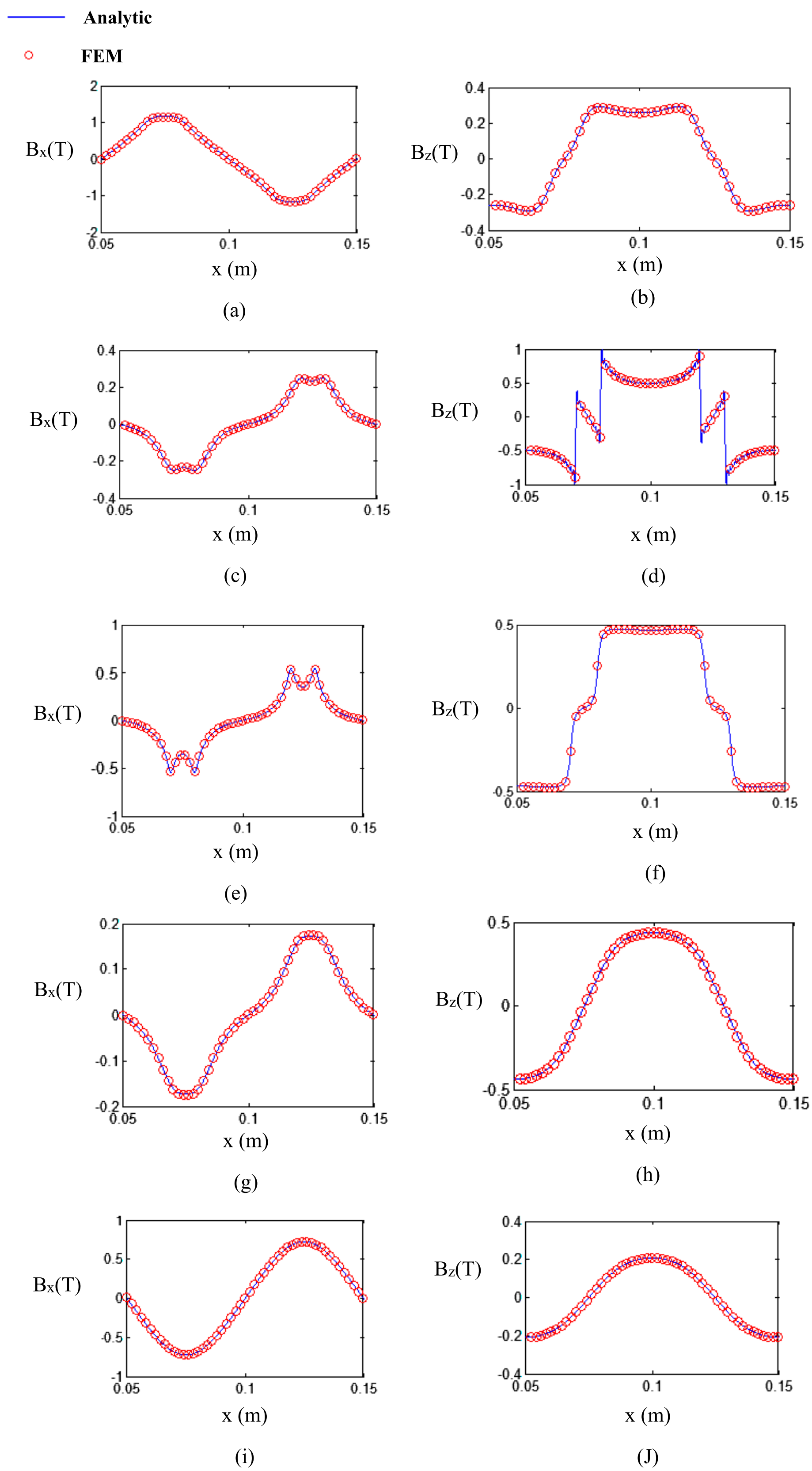

Fig. 5 Distribution of flux density for parallel magnetization: **a** Flux density horizontal component of FR, **b** Flux density vertical component of FR, **c** Flux density horizontal component of FPM, **d** Flux density vertical component of FPM, **e** Flux density horizontal component of FAG, **f** Flux density vertical component of FAG, **g** Flux density horizontal component of FW, **h** Flux density vertical component of FW **I** Flux density horizontal component of S **J** Flux density vertical component of S, **k** Flux density horizontal component of SW **L,** Flux density vertical component of SW, **m** Flux density horizontal component of SAG, **n** Flux density vertical component of SAG, **o** Flux density horizontal component of SPM, **p** Flux density vertical component of SPM, **Q**) Flux density horizontal component of SR, **R** Flux density vertical component of SR

Fig. 5 continued

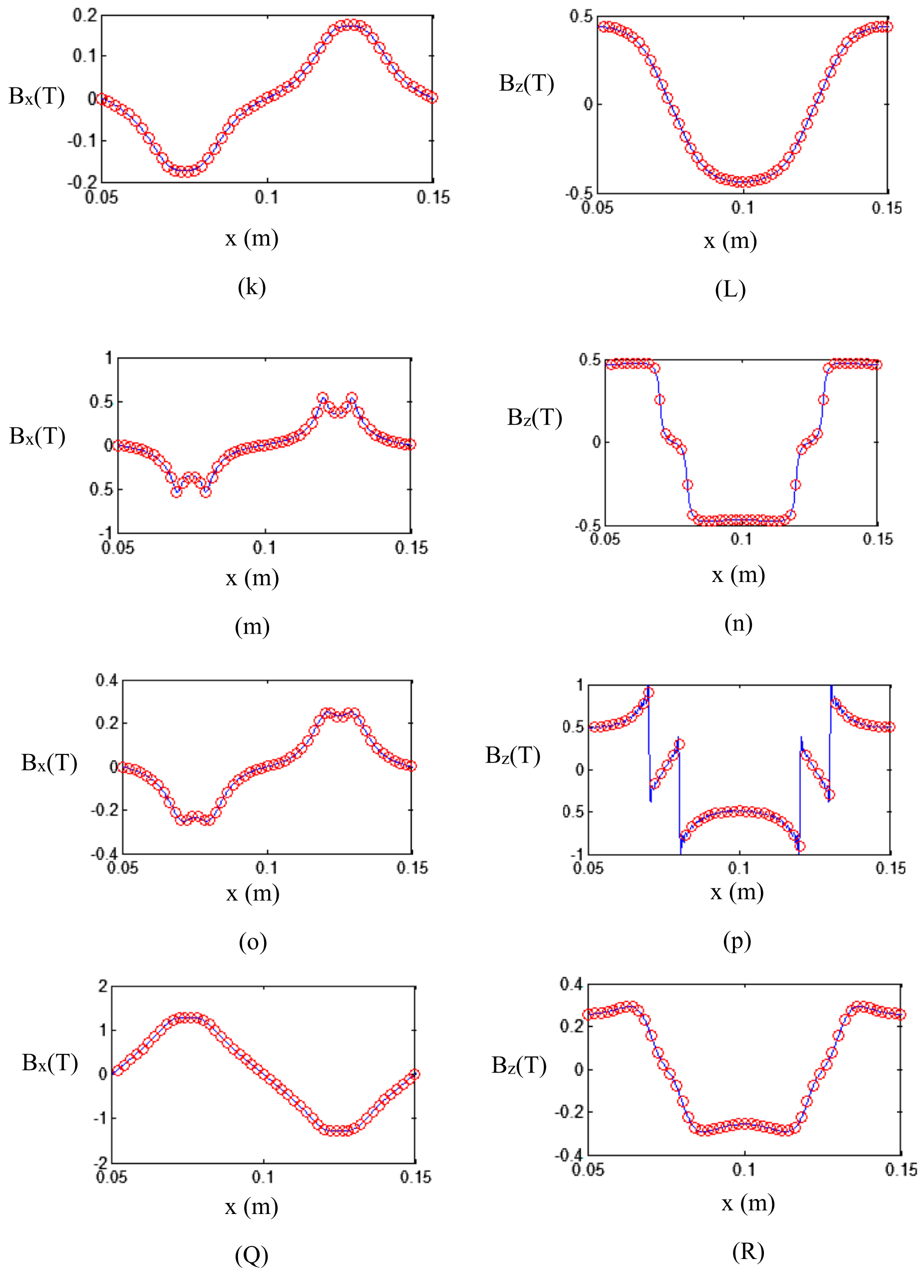

4 Conclusion

This paper concentrated on analytical model to calculate magnetic flux density for LPMIADSSMs. Sub-domain method based on partial differential equations is applied due to its accuracy and speed of obtaining answers, and by this model, the effects of AR and PMs with different magnetization patterns on distribution of flux density in all sub-regions are scrutinized. Finally, the results for both PM and AR are validated by FEM extracted by Maxwell software.

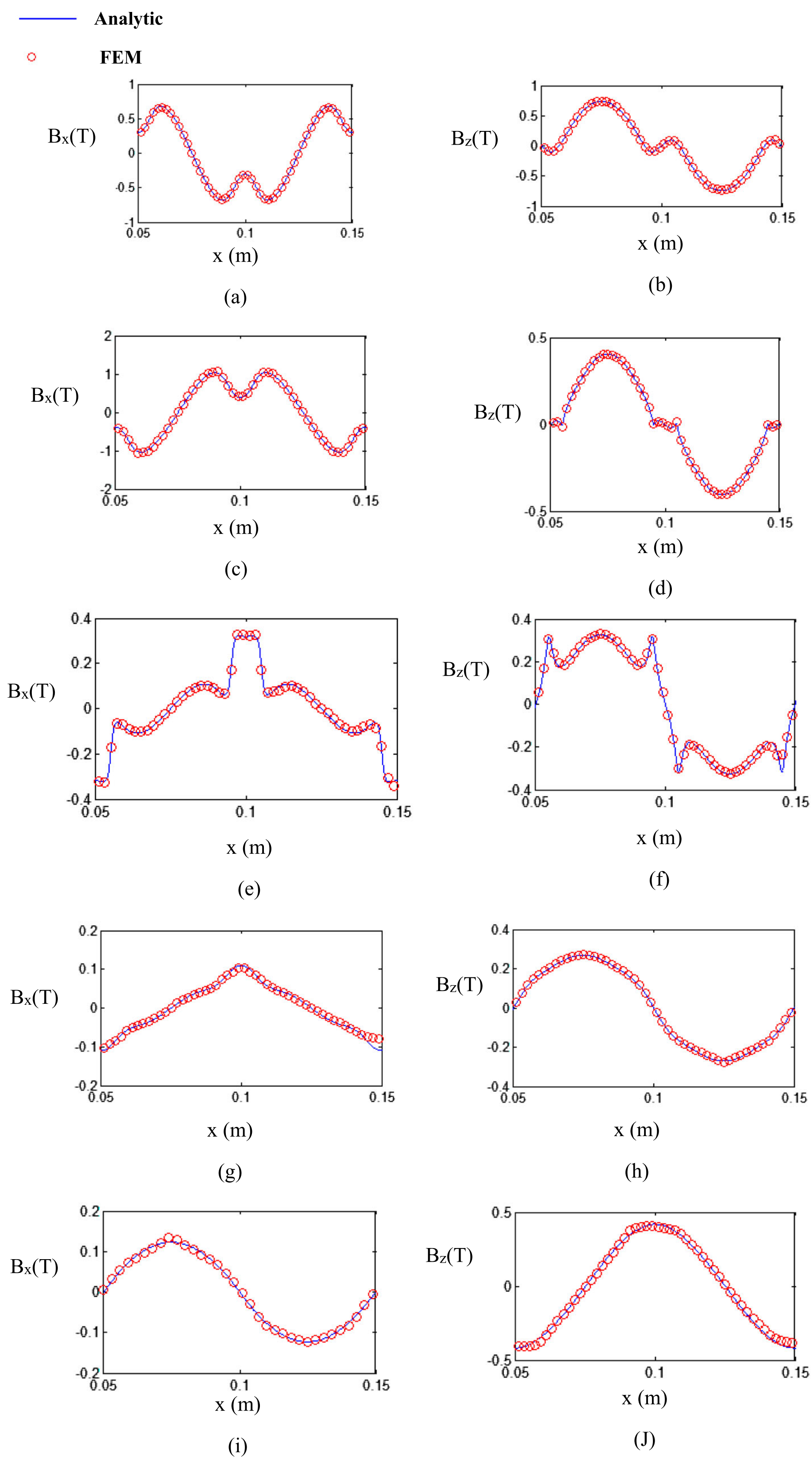

Fig. 6 Distribution of flux density for bar magnet in the shifting direction magnetization: **a** Flux density horizontal component of FR, **b** Flux density vertical component of FR, **c** Flux density horizontal component of FPM, **d** Flux density vertical component of FPM, **e** Flux density horizontal component of FAG, **f** Flux density vertical component of FAG, **g** Flux density horizontal component of FW, **h** Flux density vertical component of FW, **I** Flux density horizontal component of S, **J** Flux density vertical component of S, **k** Flux density horizontal component of SW, **L** Flux density vertical component of SW, **m** Flux density horizontal component of SAG, **n** Flux density vertical component of SAG, **o** Flux density horizontal component of SPM, **p** Flux density vertical component of SPM, **Q** Flux density horizontal component of SR, **R** Flux density vertical component of SR

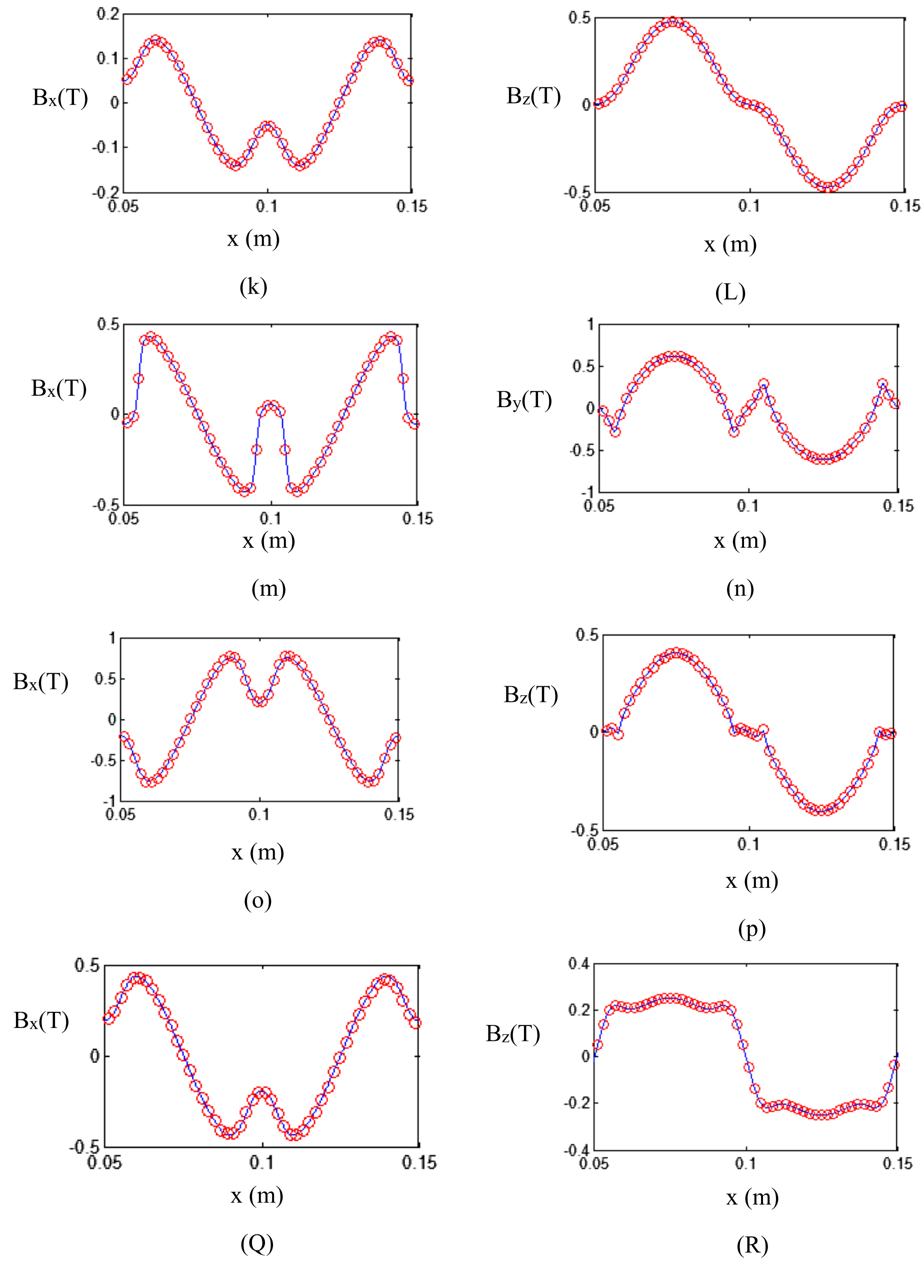

Fig. 6 continued

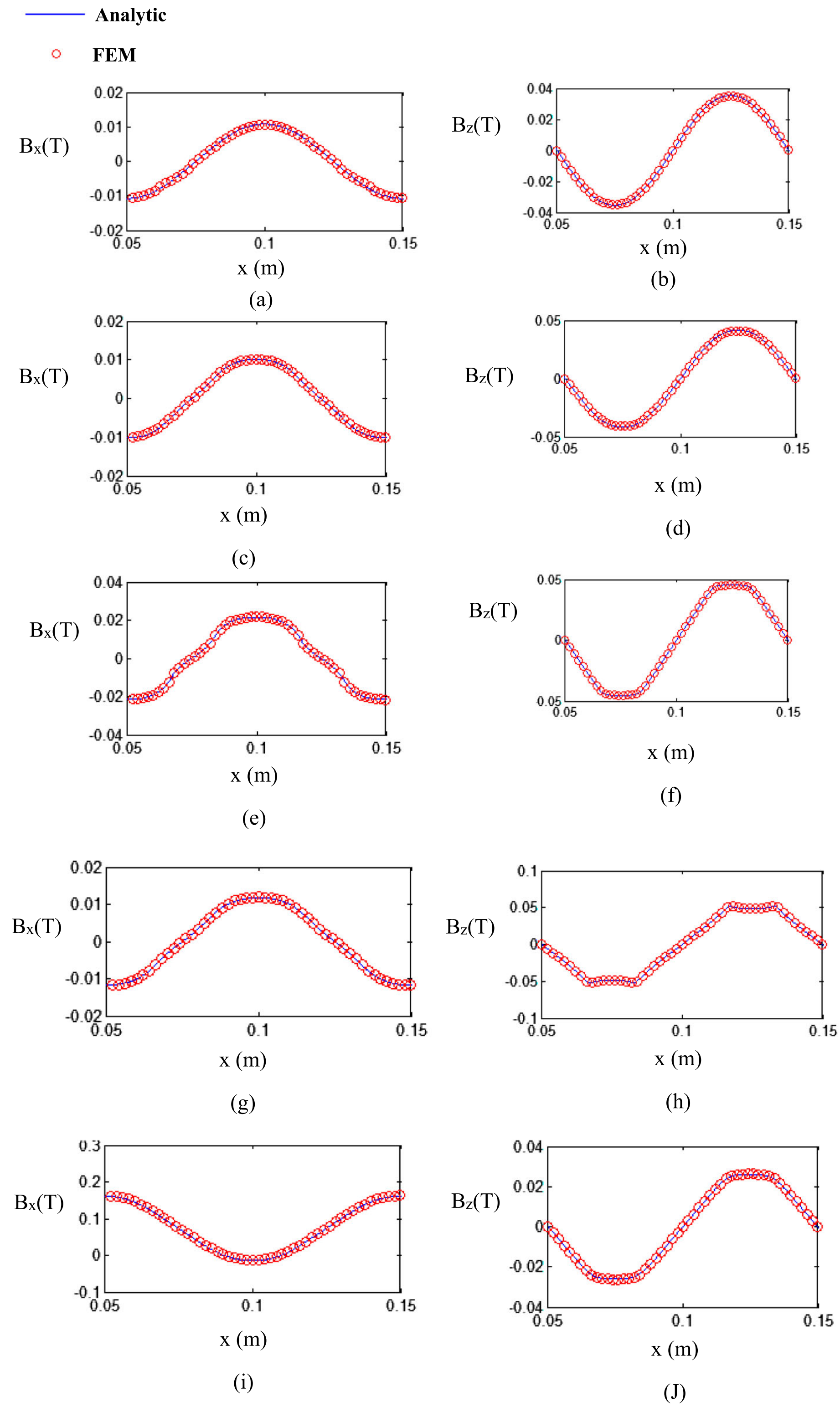

Fig. 7 Distribution of flux density for only AR: **a** Flux density horizontal component of FR, **b** Flux density vertical component of FR, **c** Flux density horizontal component of FPM, **d** Flux density vertical component of FPM, **e** Flux density horizontal component of FAG, **f** Flux density vertical component of FAG, **g** Flux density horizontal component of FW, **h** Flux density vertical component of FW, **I** Flux density horizontal component of S, **J** Flux density vertical component of S, **k** Flux density horizontal component of SW, **L** Flux density vertical component of SW, **m** Flux density horizontal component of SAG, **n** Flux density vertical component of SAG, **o** Flux density horizontal component of SPM, **p** Flux density vertical component of SPM, **Q** Flux density horizontal component of SR, **R** Flux density vertical component of SR [16]

Fig. 7 continued

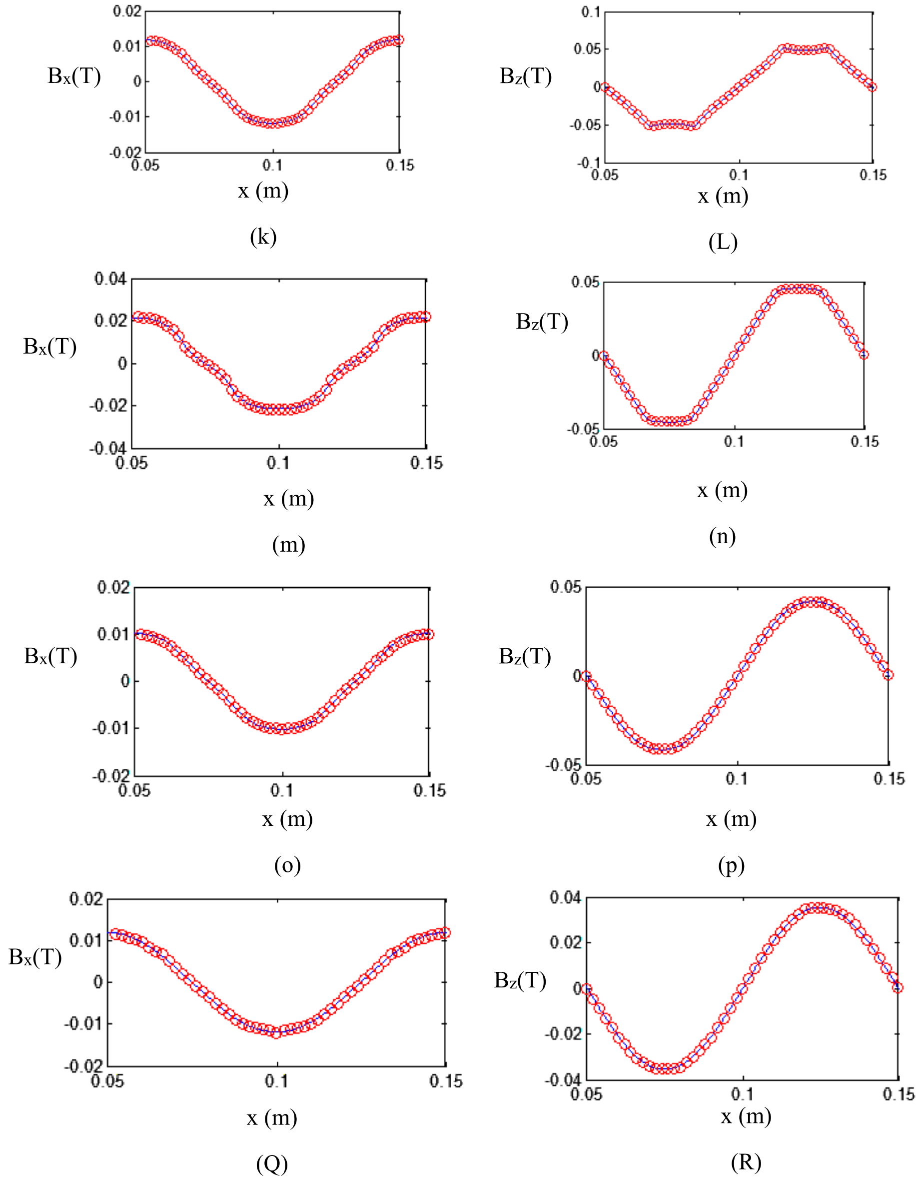

Author contributions The authors confirm the contribution to the paper as follows: First and second authors performed study conception and design; first author collected the data; First, second and third author did analysis and interpretation of results; second and third authors done draft manuscript preparation.

Funding This research received no specific grant from any funding agency in the public, commercial, or not-for-profit sectors.

Data availability No datasets were generated or analyzed during the current study.

Declarations

Conflict of interests This research is sponsored by [Bojnourd University] and may lead to development of products.

Ethical approval I hereby declare that this thesis represents my own work which has been done after studying at university of Bojnourd, and has not been previously included in a thesis or dissertation submitted to this or any other institution for a degree, diploma or other qualifications. I have read the research ethics guidelines, and accept responsibility for the conduct of the procedures in accordance with Springer journal. We confirm that we have given due consideration to the protection of intellectual property associated with this work and that there are no impediments to publication, including the timing of publication, with respect to intellectual property. In so doing, we confirm that we have followed the regulations of our institutions concerning intellectual property. We further confirm that any aspect of the work covered in this manuscript that not has involved either experimental animals or human patients. We understand that the Corresponding Author is the sole contact for the Editorial process (including Editorial Manager and direct communications with the office). We confirm that we have provided a current, correct email address which is accessible by the Corresponding Author.

References

1. D Fu, K Wu, X Wu, Q Yu, (2021) Modeling and analysis of a flux-switching transverse-flux permanent magnet tube linear motor. *2021 13th International Sympsium on Linear Drives for Industry Applications*, article number: 21048719.
2. Zhang Z, Luo M, Duan J, Kou B (2022) Design and analysis of a novel frequency modulation secondary for high-speed permanent magnet linear synchronous motor. IEEE/ASME Trans Mechatron 27(2):790–799
3. Cui F, Sun Z, Xu W, Qian H, Cao C, (2021) Optimization analysis of a lon primary permanent magnet linear synchronous motor. *IEEE Transactions on Applied Superconductivity,* article number: 21082460.
4. Jensen WR, Pham TQ, Foster SN, (2017) Linear permanent magnet synchronous machine for high acceleration applications. *2017 IEEE International Electric Machines and Drives Conference (IEMDC)*' article number: 17083920.
5. Gerlando AD, Foglia G, Felice Iacchetti M, and Perini R, (2011) Axial flux PM machines with concentrated armature windings: design analysis and test validation of wind energy generators. *IEEE Transactions on Industrial Electronics*, vol. 58, no 9, pp 3795–3805.
6. Tiegna H, Bellara A, Amara Y, Barakat G (2012) Analytical modeling of the open-circuit magnetic field in axial flux permanent-magnet machines with semi-closed slots. IEEE Trans Magn 48(3):1212–1226
7. Egea A, Almandoz G, Poza J, Ugalde G, and Escalada AJ, (2010) Axial-flux-machine modeling with the combination of fem-2-D and analytical tools. *The XIX International Conference on Wlectrical Mchines-ICEM 2010*, article number: 11615162.
8. Mohammadi S, Mirsalim M, Vaez-Zadeh S, Talebi HA (2014) Analytical Modeling and Analysis of Axial-Flux Interior Permanent-Magnet Couplers. IEEE Trans Ind Electr 61(11):5940–5947
9. Huang Y, Ge B, Dong J, Lin H, Zhu J, Guo Y (2012) 3-D analytical modeling of no-load magnetic field of ironless axial flux permanent magnet machine. IEEE Trans Mgnet 48(11):2929–2932
10. de la Barrière O, Hlioui S, Ben Ahmed H, Gabsi M, LoBue M (2012) 3-D formal resolution of maxwell equations for the computation of the no-load flux in an axial flux permanent-magnet synchronous machine. IEEE Trans Magnet 48(1):128–136
11. Yacine A (2012) Analytical modeling of the open-circuit magnetic field in axial flux permanent-magnet machines with semi-closed slots. IEEE Trans Magnet 48:3
12. Wang K, Wang D, Lin H, Shen Y, Zhang X, Yang H (2014) Analytical modeling of permanent magnet biased axial magnetic bearing with multiple air gaps. IEEE Trans Magnet 50(11):8002004
13. Xia B, Jin MJ, Shen JX and Zhang AG, (2011) Design and analysis of an air-cored axial flux permanent magnet generator for small wind power application.*2010 IEEE International Conference on Sustainable Energy Technologies (ICSET)*, article number: 11730611, Jn.
14. Sung SY, Jeong JH, Park YS, Choi JY, Jan SM (2012) Improved analytical modeling of axial flux machine with a double-sided permanent magnet mover and slot-less stator based on an analytical method. IEEE Trans Magnet 48(11):2760–2763
15. Gerlando AD, Foglia G, Iacchetti MF, Perini R (2011) Axial flux PM machines with concentrated armature windings: design analysis and test validation of wind energy generators. IEEE Trans Ind Electr 58(9):3795–3805
16. Ghaffari A (2019) 2-D analytical model for predicting magnetic flux distribution in slotless single-sided axial flux permanent-magnet synchronous machines. J Model Opt 2019:97–105
17. Alipour A, Moalle M, (2013) Analytical Magnetic field analysis of axial flux permanent-magnet machines using schwarz-christoffel transformation. *2013 International Electric Machines& Drives Conference*, article number: 13653192.
18. Tiaraju L, Loureiro R, Filho AFF, Zabadal JRS, Homrich RP (2008) A model of a permanent magnet axial-flux machine based on lie's symmetries '. IEEE Trans Magnet 44(11):4321–4324
19. Lubin T, Mezani S, Rezzoug A (2013) Development of a 2-D analytical model for the electromagnetic computation of axial-field magnetic gears. IEEE Trans Magn 49(11):5507–5521
20. Azzouzi J, Barakat G, Dakyo B (2005) Quasi-3-D analytical modeling of the magnetic field of a axial flux permanent-magnet synchronous machine. IEEE Trans Energy Conv 20(4):7692294
21. Hong SA, Choi JY, Jang SM, Jung KH (2014) Torque analysis and experimental testing of axial flux permanent magnet couplings using analytical field calculations based on two polar coordinate systems. IEEE Trans Magnet 50(11):8205304
22. He P, Jiao Z, Yan L, Liang H, Chen CY and Chen IM, (2015) Analysis of magnet layout in circumferential and axial direction for halbach PM arrays. *Proceedings of a 2014 IEEE Chinese Guidance, Navigation and Control Conference*, article number: 14851874.
23. Parviainen A, Niemelä M, Pyrhönen J (2004) Modeling of axial flux permanent-magnet machines. IEEE Trans Ind Appl 40(5):1333–1340
24. Choi JY, Ho Lee S, Ko KJ, Jang SM (2011) Improved analytical model for electromagnetic analysis of axial flux machines with double-sided permanent magnet mover and coreless stator windings. IEEE Trans Magnet 47(10):2760–2763
25. Koechli C, Perriard Y, (2013) Analytical model for slotless permanent magnet axial flux motors. *2013 International Electric Machines& Drives Conference*, article number: 13653209.
26. Sung SY, Jeong JH, Park YS, Choi JY, Jang SM (2012) Improved analytical modeling of axial flux machine with a double-sided permanent magnet mover and slotless stator based on an analytical method. IEEE Trans Magn 48(11):2945–2948